JOURNAL OF SPACECRAFT AND ROCKETS
Vol. 41, No. 4, July–August 2004

Staged Microgravity Deployment of a Pressurizing Scale-Model Spacecraft

Jennie E. Campbell,* Suzanne Weaver Smith,† J. A. Main,‡ and Justin Kearns*
University of Kentucky, Lexington, Kentucky 40506

The experiments described were conducted with the goal of obtaining quantitative pressure and motion data for deployment of an inflatable scale-model spacecraft structure in an environment free of gravity. The experiments included a series of staged deployments of two identical unfolding, inflating scale-model solar concentrators, each consisting of three struts and a torus. The experiments were conducted aboard NASA's KC-135 aircraft. Internal pressure was simultaneously measured at six locations in the deploying structure at the bottom and top of each strut. Deployment motions were tracked using two video cameras and were compared to measured pressures. Consistent trends in pressurization and motion were seen in 11 staged deployments, including nearly constant pressure as the internal volume increased and increasing pressure as volume remained constant. Pressure equalization was observed to occur at different times for different struts, and motion analysis showed varied directions of deployment correlating to these differing pressure equalization times.

Nomenclature

f	=	distance between the focal plane and the retinal plane, in.
P	=	perspective projection matrix
P_{ij}	=	elements of perspective projection matrix
S	=	scale factor, projected coordinate to image coordinate
U	=	projected coordinate of a point, in.
u	=	image coordinate, in.
V	=	projected coordinate of a point, in.
v	=	image coordinate, in.
X	=	global coordinate of a point, in.
Y	=	global coordinate of a point, in.
Z	=	global coordinate of a point, in.

Introduction

INFLATABLE spacecraft structures are of interest because their small packaging characteristics and versatility offer unique solutions to the common aerospace challenge of maximizing performance while minimizing weight. Understanding the deployment of these structures, both experimentally and analytically, has been a topic of several recent research activities.[1–4] For example, simulations of z-folded inflatable cylindrical tubes have been conducted using nonlinear finite element programs by researchers at NASA Langley Research Center, and effects of inflation rates on the deployment dynamics (e.g., pressure vs time and volume vs time) have been analyzed.[3] Also, researchers at Nihon University in Japan have compared drop-shaft-type microgravity deployments of a single-fold inflatable tube with finite element simulations.[4]

The experiments described in this paper were conducted with the goal of obtaining quantitative pressure and motion data during the deployment of an inflatable structure in a gravity-free environment. A series of deployment experiments were conducted using two identical inflatable scale-model solar concentrators, each consisting of three struts and a torus. The test articles were one-quarter-size scale models of the Shooting Star Experiment, which demonstrated an inexpensive space propulsion system using focused energy of the sun.[§] Deployment of the test articles progressed in stages, as different sections were released. The experiments were performed in the microgravity environment on NASA's KC-135 aircraft in March 2001.

The present experimental research program followed from two previous microgravity experiments and a series of 1-g experiments to explore the deployment dynamics of inflatable structures. In the first microgravity experiment, three solar-array models and a solar-concentrator model, each constructed of inflating tubes, were videotaped while deploying in a microgravity environment.[5] All four structures showed similar characteristics including development of folds or "hinges," often with a single hinge unfolding as the final stage of deployment.

Using these results, several models of unfolding, inflating tube deployment were developed.[5,6] For verification of these models, a series of static and dynamic experiments were performed in a 1-g environment.[7] A folded tube was inflated; inlet- and far-end pressures were recorded for various tube size and fold angles, among other variables. Pressurization delays, that is, differences in pressure caused by folds in the tube in combination with size and pressure, were observed in some cases. Also, as tubes inflate and unfold during deployment, phases of constant-pressure, increasing-volume (CPIV) and constant-volume, increasing-pressure (CVIP) were observed to occur.

Quantitative information on microgravity deployment was also desired. Therefore, in the second microgravity experiment an unfolding, inflating tube was instrumented and deployed in the microgravity environment with the goal of obtaining synchronous pressure and motion data.[8] In the microgravity environment, no pressure delays were seen because strain energy in the folded tube was sufficient to unfold the tube enough to prevent pressurization delays. This characteristic was also seen in nonlinear finite element simulations of slow inflation of unfolding tubes.[3]

In the present study, a similar series of microgravity deployment experiments were conducted on a more complex inflatable structure model representing an unfolding, inflatable solar concentractor. The present paper starts with a description of the experiments, followed by presentation of pressurization results for different deployment scenarios. Then, deployment motion data, as traked using video cameras, are presented. Finally, pressurization and motion results are compared.

Received 10 November 2002; accepted for publication 23 April 2004.

*Undergraduate Research Assistant, Department of Mechanical Engineering.

†Associate Professor, Department of Mechanical Engineering. Associate Fellow AIAA.

‡Associate Professor, Department of Mechanical Engineering. Senior Member AIAA.

§Data available online at http://grin.hq.nasa.gov/ABSTRACTS/GPN-2000-000067.html and http://www.grc.nasa.gov/WWW/tmsb/secondaryconc/doc/rsc_sse.html.

Experiment Description

The primary objective of this experiment was to study the internal pressurization characteristics of the structures as it deploys in a microgravity environment from its initial, folded configuration to its final position. The secondary objective was to relate pressurization and motion for the deploying structure. The NASA KC-135 aircraft, which flies repeated parabolic flight paths to simulate a microgravity environment, was utilized for the present tests. Individual tests were conducted during 20-s periods of microgravity, which alternated between periods of 2-*g* acceleration with 10-s transition periods between.

A schematic of the experimental apparatus is shown in Fig. 1. The test article consisted of a folded Kapton structure consisting of three tubular booms leading to a torus and mounted to a base and an air pump. The lens of the solar concentrator supported by the torus was omitted for these experiments. Air from the air pump was first passed through two chambers (not shown) that smooth the flow and measure the flow rate, respectively. After passing through these two chambers, the air fed into a three-way junction in the base and finally into the three struts.

During deployment tests, internal pressure was simultaneously measured at two locations in the second chamber and at six locations in the deploying structure, which can be seen in Fig. 2. Thin flexible tubing was threaded through the base support of each strut into the interior of the structure. One tube was extended the full length of the strut, while the other remained at the bottom. External pressure sensors connected to these tubes made it possible to measure the pressure at the top and bottom of each strut. As the structure was inflated, a triaxial dc accelerometer mounted near the base sensed the microgravity environment. Images simultaneously recorded by two orthogonal video cameras allow reconstruction of three-dimensional motion by tracking visual targets. This enables analysis of position, velocity, and acceleration during deployment to compliment the pressurization data.

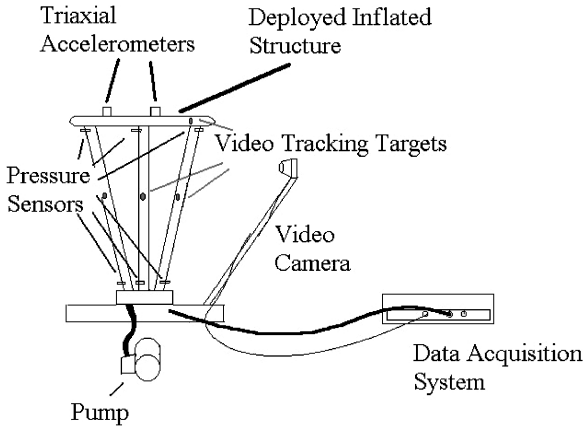

Fig. 1 Experiment schematic.

The instrumented test article on the KC-135 is shown in Fig. 3. The test article is mounted to a stiff sandwich-plate support that is securely strapped to the floor of the KC-135. Black and white tracking targets are seen on the struts and torus. Black camera-support arms extend to the left and directly behind the structure; transparent grids with gray frames are mounted directly in front of the cameras.

The experiment progressed with one period of microgravity used to deploy the test article and the next period of microgravity used to refold and secure it. First, the air pump was reversed, and sections of the structures were flattened to remove as much residual air as possible. The test article was hand-folded at predefined locations along the struts and torus using z-folds (a map-folding pattern). As it was folded, three straps fastened with electromagnets secured the structure. When the plane entered a microgravity period, the magnets were released in sequence, at about 1-s intervals, releasing the structure in stages from the base up. The first strap secured the entire folded structure, the second released folds in the struts, and the final one released the folded torus.

The experiment was conducted during two flight days. A different test article was used on each days so that detrimental effects of repeated deployments were minimized. Overall, 11 staged deployments were successfully recorded, along with two additional deployments having staged release but no pressurization and having pressurization without staging the release.

Figures 4 and 5 show two deployment sequences in microgravity. In Fig. 4, the deployment is staged without pressurization, that is, the pressurization occurs after all straps are released. In Fig. 5, the deployment is staged while the structure is inflating. Comparing the

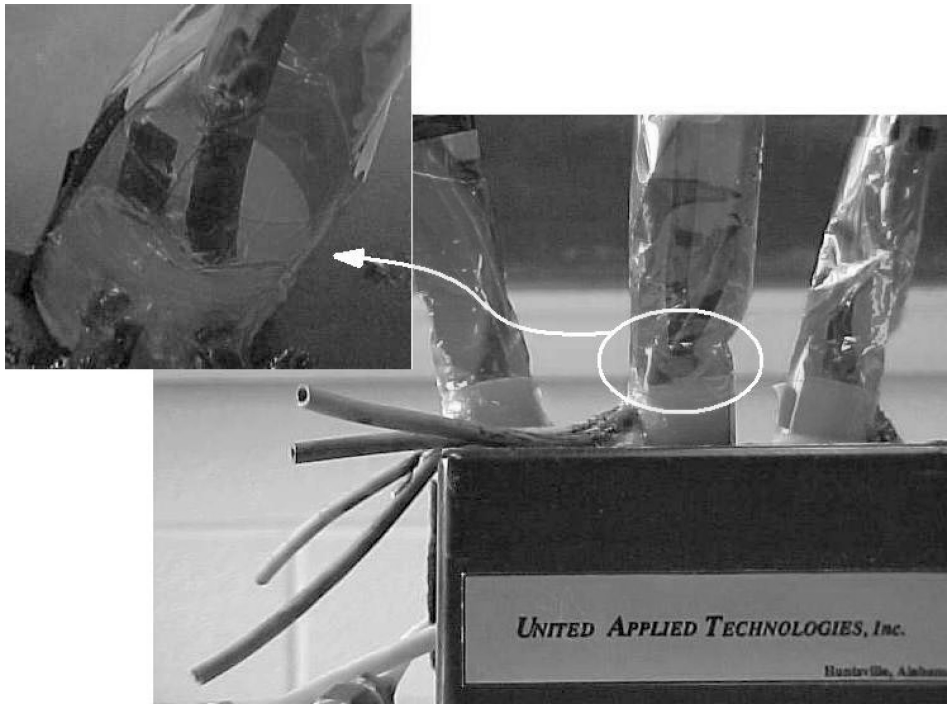

Fig. 2 Tubing and pressure sensor locations for struts.

Fig. 3 Experiment on the KC-135.

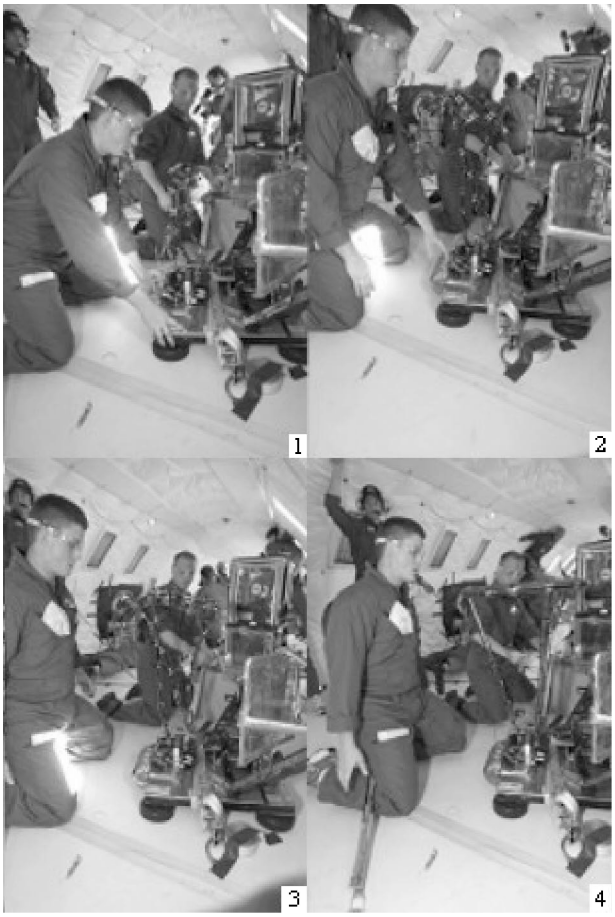

Fig. 4 Deployment sequence with staged release before pressurization.

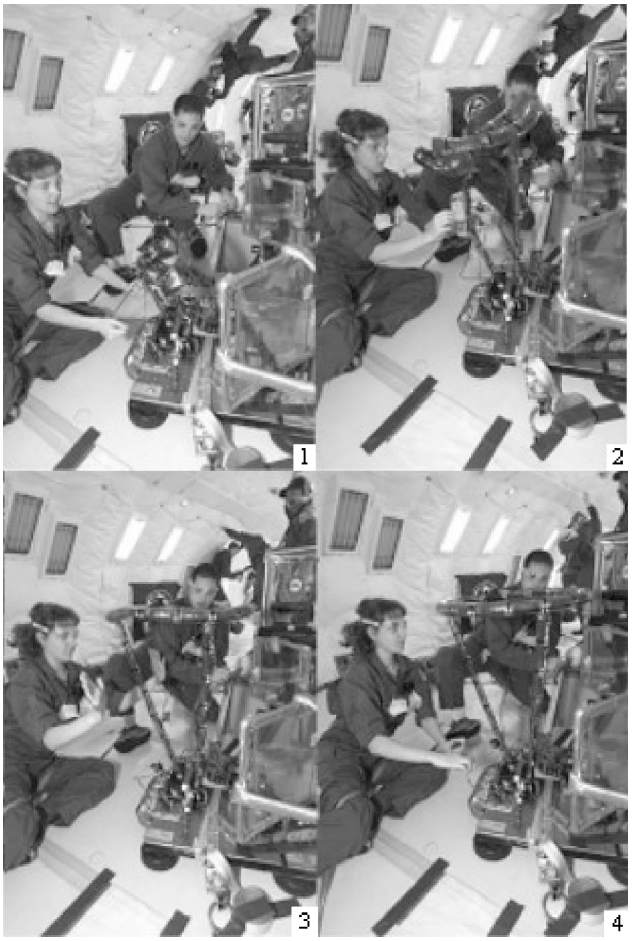

Fig. 5 Deployment sequence with staged release during pressurization.

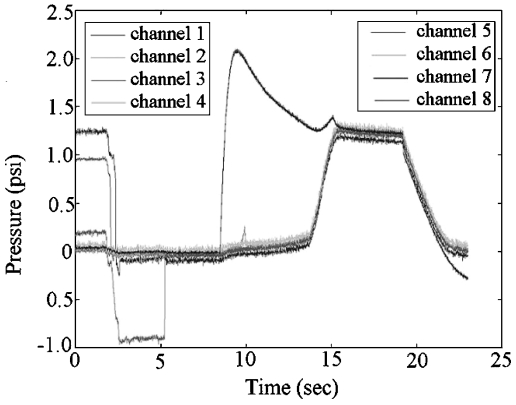

Fig. 6 Pressure time histories for deployment with pressurization after staged release: pressure data for controlled deployment with value off.

third frames of each sequence, the struts are not fully inflated in Fig. 4 as the torus is unfolding, but they are fully inflated in Fig. 5.

Pressurization Results and Comparison

Figure 6 is a plot of pressure time histories for the eight measured pressure channels for one deployment. Channels 1, 3, and 5 are internal pressure measurements at the top of the struts; channels 2, 4, and 6 are at the bottom of the struts. Channels 7 and 8 are pressure measurements at two positions in the second flow chamber, providing the pressure entering the base of the test article.

The data in Fig. 6 are from the deployment shown in Fig. 4 with staged release of the structure before pressurization. Examining this deployment scenario allows understanding of pressurization and

motion behavior for a simpler inflating system before considering staged deployments with pressurization. Pressurization of the structure is started at 8 s when the flow valve was opened. The pressure in the second chamber (and the inlet to the structure) increases rapidly to over 2 psi at 10 s and slowly decreases as the structure inflates equalizing with the structure at 16 s. The pump is reversed at 20 s, rapidly depressurizing the structure.

In Fig. 6, after 6 s, internal pressures in the structure are essentially all equal because release and unfolding of the structure occur prior to starting the pressurization. Two distinct regions are seen during the inflation from 8 to 16 s: 1) a near CPIV region between 8 and 14 s in which the structure expands to its full volume, and 2) a CVIP region between 14 and 16 s in which the internal pressure of the structure increases to equal the entering pressure.

Pressure changes are also seen during the staged release prior to inflation in Fig. 5. Initial pressures at the bottom of the struts are near zero, matching the atmospheric pressure, but the three pressures at the top of the struts (channels 1, 3, and 5) are nonzero. Even though a vacuum was applied to the structure at the base to remove air before folding, some residual air was trapped at the top of the struts. These pressures remain constant until the first electromagnet release at 2 s, and then drop as the internal volume is suddenly increased. The top and bottom pressures in two of the struts equalize when the second stage is released at 2.5 s, while the pressure in the third strut equalizes with the final release at 5 s.

Posttest calibration of the six internal pressure sensors was performed, along with other tests, to answer questions regarding the negative pressures. Nominally, the pressure gauges have a sensitivity of 100 psi/V. Posttest calibration for each pressure sensor resulted in the sensitivities listed in Table 1.

The calibration results were applied to the data of Fig. 6 to produce the pressure time histories seen in Fig. 7. Final pressures now appear to have differences not seen in the raw data shown in Fig. 6. Note that pressure differences at the start of deployment among channels 2, 4, and 6 (at the base of the struts) were constant throughout deployment, thus causing the apparent spread of pressures at the end of deployment. Pressures at the tops of the struts recorded in channels 1, 3, and 5 equalized after 5 s when the structure unfolded and then remained consistent throughout the remainder of the deployment.

Table 1 Result of calibration of pressure, sensors

Pressure sensor	Calibration correction factor, psi/V	Zero factor, psi
1	108.37	0.0436
2	109.62	−0.8660
3	105.38	0.0172
4	118.45	0.1524
5	105.62	−0.0045
6	116.00	−0.0626

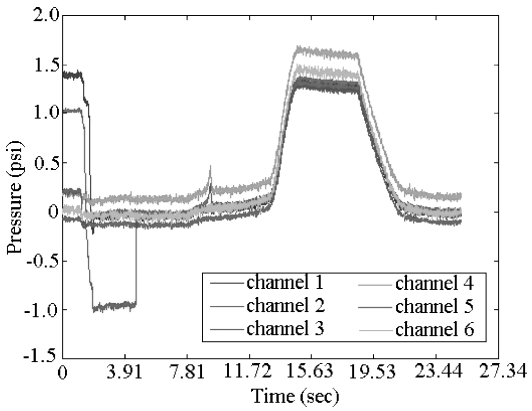

Fig. 7 Calibrated pressure time histories for deployment with pressurization staged release: corrected pressurization data for a controlled deployment with value off.

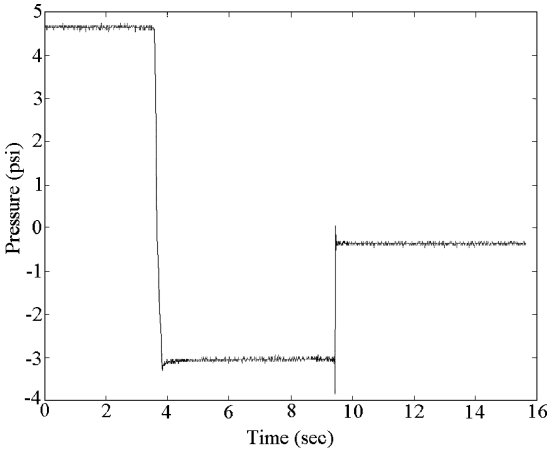

Fig. 8 Posttest calibration data to explain negative pressure drop.

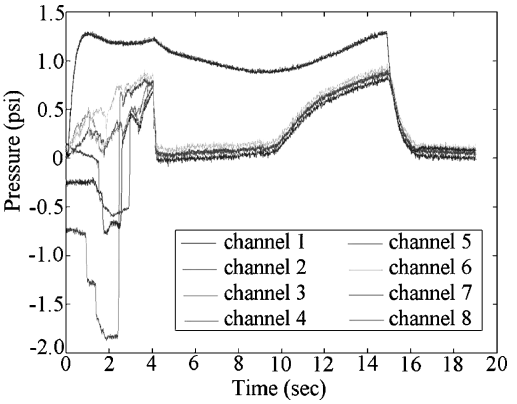

Fig. 9 Pressure time histories for deployment with pressurization during staged release: pressurization data for a controlled deployment with value on.

Typically one of the three struts showed negative pressure readings during deployment. Figure 8 presents time-history data from a pressure sensor connected to a syringe. The syringe was first half filled with air and attached to a closed tube including the pressure sensor. The plunger of the syringe was then depressed completely to provide an initial positive pressure. This pressure was held for 4 s. The plunger was then retracted to the full extent of the syringe and held for the next 5 s. The increase in system volume, over that of the initial (half-syringe) volume, led to negative pressure readings because the internal pressure in this system was less than atmospheric during this time. Finally, the plunger was removed completely, opening the system and returning the pressure reading to zero. This same behavior is seen in many of the deployment pressure results. How this relates to the unfolding structure will be discussed further in the Motion and Pressure Comparison section.

Figure 9 presents typical pressure time histories for a deployment with staged release and pressurization occurring simultaneously. Pressurization starts just after 0 s as seen in channels 7 and 8. When the valve is opened, the entering pressure increases rapidly to 1.25 psi, and remains greater than 1 psi until the valve is closed at 15 s. After the final release at 4 s, inflation of the structure includes the same regions seen before, CPIV then CVIP. These regions consistently appear in every deployment. The structure's final internal pressure is not equal to the entering pressure in this case because the test is stopped at 15 s before equalization occurs.

In Fig. 9, during the staged release portion of the deployment between 0 and 4 s, residual pressure is again seen at the top of the struts (channels 1, 3, and 5). As in the preceding unpressurized deployment, these residual pressures drop dramatically with the suddenly increased volume from release of the structure, but then equalize with the bottom strut pressures as the third release occurs.

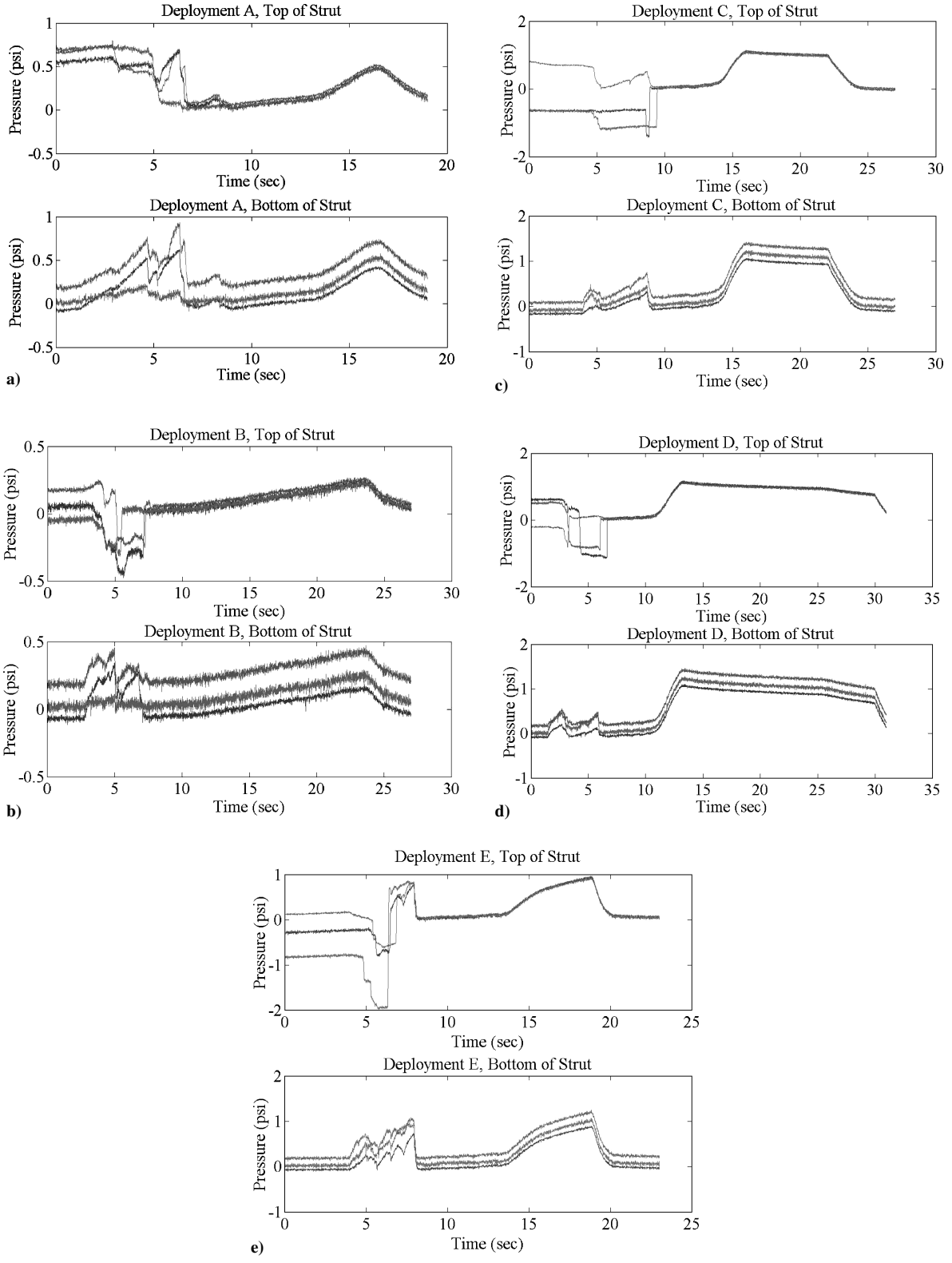

Fig. 10 Five deployments showing common pressure characteristics.

Pressures at the base of the structure (channels 2, 4, and 6) clearly show the staged release. These pressures increase until 1 s when the first release occurs. The bottom strut pressures then drop with increased internal volume. These pressures increase again, and then drop suddenly, with subsequent releases at 3 and 4 s.

Similar characteristics were seen among the pressurization histories of the 11 staged deployments of the two inflating structures. In Fig. 10, results from five of these deployments show this consistency. Two subplots are included in each of Figs. 10a–10e. The top subplot is of the pressures at the tops of the struts; the bottom subplot is of the pressures at the bottom of the struts.

Every deployment included regions of CPIV and CVIP after release of the final stage. These five deployments also show constant differences among the bottom strut pressures, which matches the differences at the beginning of the deployment, once final pressure is reached. As the struts completely unfold, their top and bottom pressures equalize. All deployments show one strut pressure equalizing after the other two. However, it is not always the same strut.

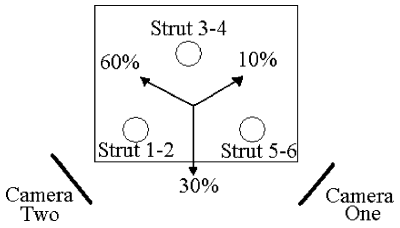

Fig. 11 Initial deployment statistics.

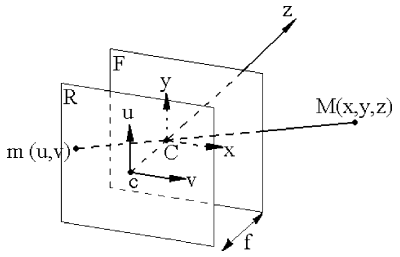

Fig. 12 Pinhole camera model.[9]

Motion analysis shows the structure initially deploying to one side even without the presence of gravity, but it is not always the same side. Approximately 60% deployed between struts 1-2 and 3-4 first, while 30% deployed between struts 1-2 and 5-6 and the other 10% between struts 3-4 and 5-6, with the numbers here referring to the corresponding pressure channels at the top and bottom of the struts. These are depicted schematically in Fig. 11. Analysis of the recorded motion data suggested the direction of the last z-fold near the base of the structure determines the direction of deployment, whereas lagging pressure equalization only represents the last strut to fully deploy, independent of deployment direction.

Motion Analysis

As seen in Fig. 3, two orthogonal video cameras were included to record the motion of the inflating structure. Motion analysis proceeded from analysis of a single two-dimensional view to three-dimensional reconstruction. Prior to comparison with the pressure results, the recorded motion data must be calibrated to be in a functional form. Calibrating the recorded images also leads to the ability to construct a three-dimensional model of the deployment. Black and white cross-hair targets were mounted on each leg and around the torus. These target dots are the points of interest for tracking and in the reconstruction of the motion.

The physical model of a pinhole camera that is seen in Fig. 12 consists of a focal plane parallel to a retinal plane. The focal plane contains the optical center of camera. The retinal plane, located a distance f behind the focal plane, contains the image created by linear projections from points on the three-dimensional object through the optical center. The distance f is referred to as the focal distance of the camera. The operation of forming an image on the retinal plane is called perspective projection.[9]

The linear relationship between the projected coordinates of a point in the retina and the object coordinates in the global coordinate system[9] is

$$\begin{Bmatrix} U \\ V \\ S \end{Bmatrix} = \begin{bmatrix} P_{11} & P_{12} & P_{13} & P_{14} \\ P_{21} & P_{22} & P_{23} & P_{24} \\ P_{31} & P_{32} & P_{33} & P_{34} \end{bmatrix} \begin{Bmatrix} X \\ Y \\ Z \\ 1 \end{Bmatrix} \tag{1}$$

The relationships between U, V, and S and u and v are[9]

$$u = U/S, \qquad v = V/S \qquad \text{if} \qquad S \neq 0 \tag{2}$$

If the global coordinates and the image coordinates are known at six nonplanar points, the unknown variables ($P_{11}, P_{12}, \ldots, P_{34}$) in the perspective projection matrix P, which represent the intrinsic and extrinsic parameters of the given camera, can be determined. Determination of these parameters is referred to as camera calibration.

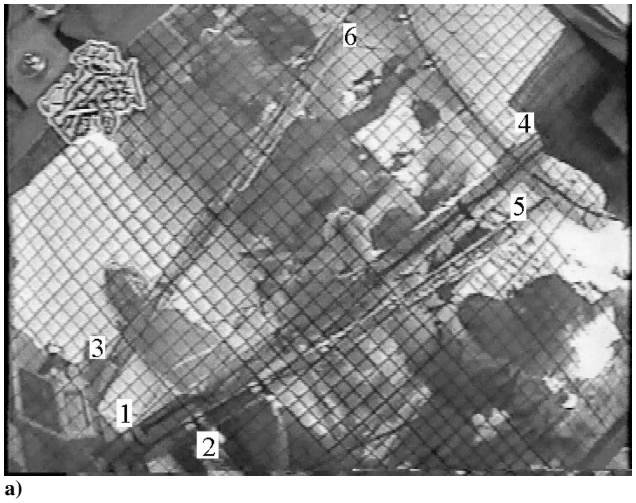

a)

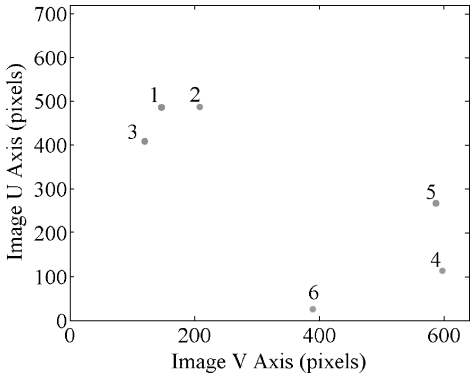

b)

Fig. 13 Captured frame from camera one and the corresponding tracked image.

For camera calibration, the top and bottom tracking point of each fully inflated strut were used, resulting in the required six points. Their global positions were measured relative to an origin defined at one corner of the optical bench. To define the image coordinates required the conversion of the VHS video frames to a sequence of digital pictures. VHS recording captures motion at 30 frames per second (fps). Once the video is digitized, the software used allows the frames to be captured at different speeds (e.g., 12, 8, and 2 fps), thus creating a slide-show presentation of a moving system at nearly identical time intervals. Software used for the tracking process consisted of a program that automatically loaded consecutive frames and recorded the sequence of manually selected points. Figure 13 presents a captured video frame of the fully inflated test article as seen from camera one and its corresponding tracked image of the six calibration points. A similar set of images can be made from camera two.

Wide-angle lenses were used for the experiment to provide the widest possible field of view. Lenses distort the image, though, as seen near the edges in Fig. 13a. A pinhole camera model does not allow for wide-angle lens distortion, so that the tracked image data had to be adjusted to correct for this distortion before deriving the projection matrix. The transparent grids mounted in front of the lenses were used for the adjustment. The grid lines provided an ample number of points for correction of the distortion of each individual camera. In addition, the cameras were mounted rotated at approximately 45 deg to provide the best views of the deploying structure.

For each camera, the tracked data set was corrected from a distorted, rotated local axis to a corrected image axis using the following procedure. First, frames were captured as jpeg images using iMovie 2 and points were tracked in pixels. These points were converted from pixels to inches using a 72 pixels/in. conversion

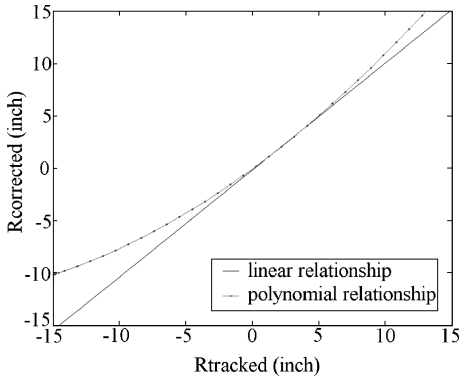

Fig. 14 Linear and second-order polynomial for converting $r_{corrected}$ from $r_{tracked}$.

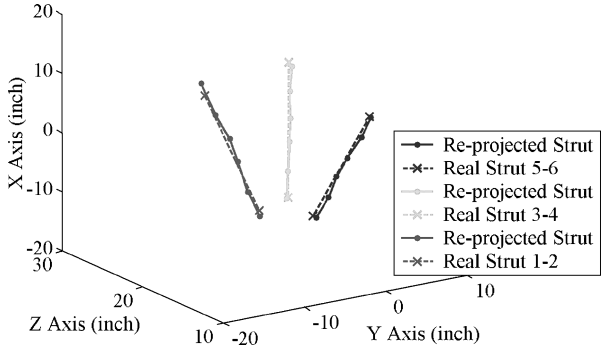

Fig. 15 Comparison plot of three-dimensional reprojected and original tracking dot locations of fully inflated struts from camera one coordinate system.

factor. Second, for each camera selected, a point where distortion was minimal at the center of the image was picked to be the calibration center. The origin of the tracked coordinates was at the corner of the frame. The tracked coordinates were translated to reference the new origin at the calibration center. Third, assuming the distortion was only radially dependent, that is equal in concentric rings around the calibration center, the u–v position data were converted into a radial position. Fourth, relating r tracked to r real for 34 transparent grid intersections, the correlation closely approximated a second-order polynomial, as expected. For smaller r values, a linear relation is adequate as seen in Fig. 14. Because the range of the tracked deployment data was within the linear approximation range, corrected r values were determined for camera one and camera two using these linear factors. Fifth, assuming that no angular distortion occurred, from the geometry of similar triangles corrected (u, v) points were determined from the corrected r values and tracked angles. Sixth, the tracking dot at the base of strut 3-4 was established as a common three-dimensional origin. The corrected (u, v) points were translated to reference this three-dimensional origin. Seventh, the original video data from both lenses were recorded at approximately a 45-deg angle to allow for more viewing area along the length of the struts. A rotation matrix was applied to the corrected (u, v) data to give the final standard u–v axis.

Equation (1) was then applied with the corrected-tracked image coordinates u and v, along with the global coordinates of the six known points, to determine the P matrix for each camera. The three-dimensional reprojection of a specific point on the structure is accomplished by combining the global coordinates resulting from applying the P matrices of the cameras to the (u, v) target points from their respective images.

Figure 15 graphically presents the error associated with the reprojection of the pair of two-dimensional images to a three-dimensional model. The reprojection of the original six points used for calibration were within an average radius of 0.9616 in. of their known global locations, with a standard deviation of 0.8301 in. These six

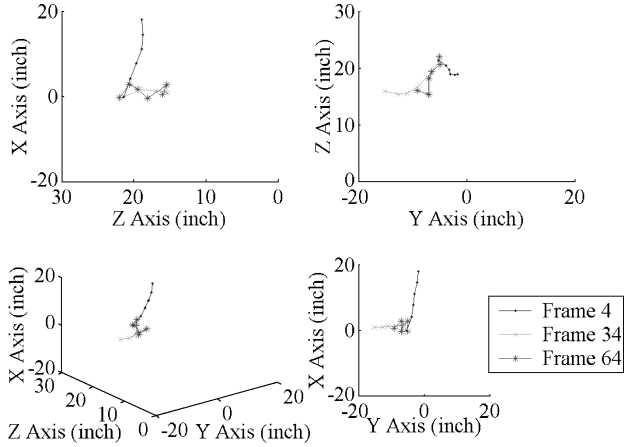

Fig. 16 Sequence of frames from the three-dimensional projection movie.

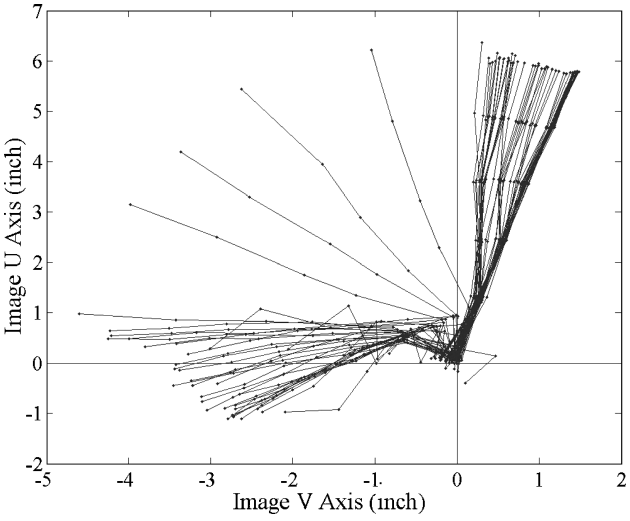

Fig. 17 Corrected motion of strut 3-4 of deployment C as seen from retinal plane of camera one (93 frames captured at 8 fps).

points, along with the remaining tracking points on each leg, were reprojected from static images of the fully developed structures. These reprojected points where plotted along with the original six points in Fig. 15.

It has been shown that a pair of two-dimensional images can be combined to determine the three-dimensional coordinate of points on the structure in the images. With the sequence of captured images from a microgravity experiment, a movie of the three-dimensional motion of the deployment can be developed. Using MATLAB 6.1, the reprojected tracked motion of each captured frame of deployment "C" was combined in an AVI movie file. Figure 16 presents a few frames of motion from this video. The power of having a three-dimensional movie of the deployment is the ability to convert position-time information to velocity and acceleration information to validate simulations, while being able to visualize the motion from any angle.

Motion and Pressure Comparison

Figure 17 presents the final tracked motion results of a film capture sequence of deployment C of strut 3-4 as seen by camera one. For simplicity, Fig. 17 represents the sequence of motion as seen from the retinal plane. For this sequence there were 93 frames captured, equivalent to 11.625 s. Each line on this graph represents one frame, approximately 0.125 s apart. The corresponding pressurization data are plotted in Fig. 18.

From the tracked video data, it can be seen that there are four different and distinct phases of deployment. Phase one corresponds

to unfolding of the z-folded structure. Phase two includes only small motions, with the test article resting in one position and its struts fully extended to the side with one 90-deg fold near the base. This phase of deployment with the development of a single final fold or hinge in an inflating tube was seen in previous experiments.[1,3]

Phase three corresponds to the struts rotating to a fully upright position as the hinge at the base unfolds. Phase four also included little or no motion of the strut, but now with the strut fully extended and the structure upright. Similar phases are seen in the tracked motion of struts 1-2 and 5-6 for this same deployment (C). For a better view of the distinct phases of deployment, Fig. 17 is separated into four subplots in Fig. 19.

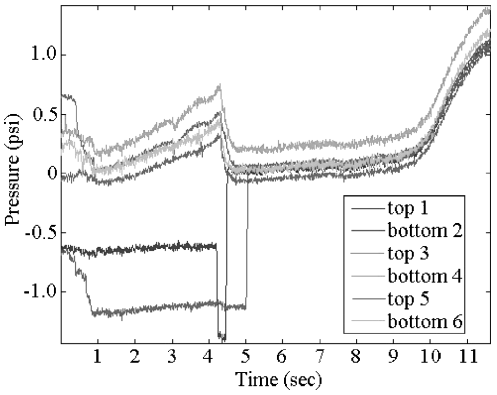

Fig. 18 Pressure data of struts 1-2, 3-4, and 5-6 of deployment C.

The motion of this deployment can now be compared to the pressure data recorded for this deployment. As just stated, one benefit of being able to capture video is the ability to have a snapshot of the motion at a certain instant in time. From Fig. 19, times of each phase were determined based on the number of frames contained in each subplot. Markers were added on the pressure plot at these times. Figure 20 shows the timing of each deployment phase and the corresponding pressure data.

Combination of all three results—pressure, video, and tracked motion—results in a generalization of the four regions the inflatable structure experiences as it inflates. Phase one corresponds to the z-fold of the strut being released and unfolded. The pressure in this region experiences a decrease because the volume is suddenly increased upon structure expansion. Phase two corresponds to the first pressure increase. Although the torus has not yet expanded, most of the volume of the struts has. Even though a bend in the structure at the base of the struts keeps them from being completely deployed, the volume of the legs is no longer increasing, thus the pressure graph represents a CVIP region. At the beginning of phase three, the electromagnet holding the strap constraining the torus is released. This corresponds to sudden increase in volume and thus

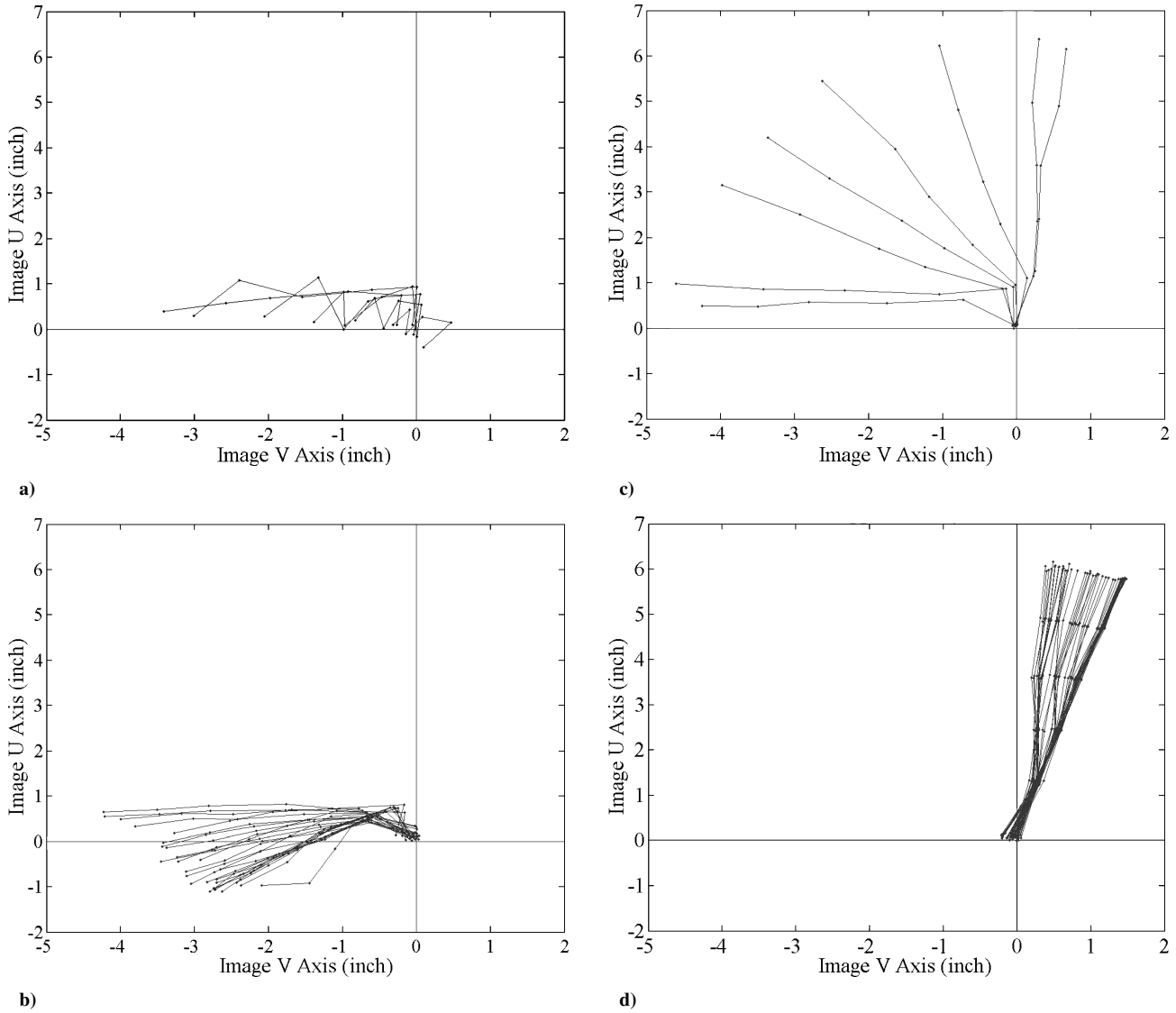

Fig. 19 Deployment C displayed in four distinct phases: a) phase one (6 frames, approximately 0.75 s), b) phase two (27 frames, approximately 3.375 s), c) phase three (8 frames, approximately 1 s), and d) phase four (52 frames, approximately 6.5 s).

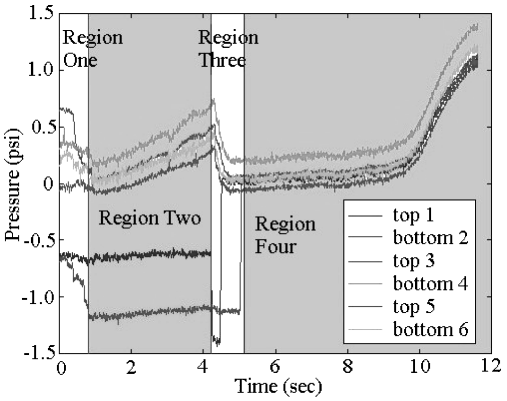

Fig. 20 Pressure deployment C showing four distinct regions.

a sudden decrease in pressure. It is in this phase that the negative pressure measurements as described in the Pressurization Results and Comparison section were seen. The release of this negative pressure to return the pressure reading to zero is the newly expanded volume increasing, thus leading to a CPIV region that is the start of phase four. This phase is achieved, and then increasing pressure occurs until the final pressure is reached.

Conclusions

Deployment of inflating space structures is a complex and nonlinear process in which the motion affects the pressurization and the pressurization affects the motion. The present study is the most recent in a series of microgravity experiments that have been conducted to explore the relationships between pressure and motion for inflating tubes and tubular structures. This study was focused on microgravity deployment experiments conducted on two solar concentrator models consisting of three inflatable tubes leading to a torus.

Deployment of the solar-concentrator models was controlled through staged releases of folded sections of the inflatable tubes. Pressurization time histories show generally consistent inflation characteristics over multiple deployment cycles including constant-pressure increasing volume and constant-volume increasing pressure after all stages are released. Variations such as side deployments and lagging pressure equalization are attributed to fold inconsistencies.

A technique for reconstructing the three-dimensional motion from two orthogonal cameras was demonstrated. Using this technique, it is possible to study the deployment from any angle, which can lead to more knowledge of how such structures deploy. In particular, it was shown that the inflatable tubes deploy in four phases, with the second phase involving the development of a single final fold or hinge as seen in previous experiments on single inflatable tubes. Pressure equalization was observed to occur at different times for different tubes, and motion analysis showed varied directions of deployment correlating to these differing pressure equalization times.

It is hoped that the results presented herein provide a better understanding of how to achieve controlled deployment of inflatable structures while also providing data that can be used for validation of analytical models for predicting deployment of these systems.

Acknowledgments

The experiment would not have been possible without generous support, contributed hardware, and extracurricular effort. We appreciate the support of the Kentucky Space Grant Consortium, Richard Hackney, Director, and of University of Kentucky Vice Chancellor for Research Jim Boling. Test articles were provided by United Applied Technologies, Inc., of Huntsville, Alabama, Rodney Bradford, President. Courtney Byers, Justin Kearns, Dustin Elliott, and Bobby Jones performed the experiment on the KC-135, with Mike Curry and Jennie Campbell as ground crew. Our appreciation is also extended to the NASA 2001 Student Flight Opportunities Program.

References

[1]Smith, S. W., and Main, J. A., "Modeling the Deployment of Inflating Space Structures," *Gossamer Spacecraft: Membrane and Inflatable Structures Technology for Space Applications*, edited by C. H. M. Jenkins, AIAA, Reston, VA, 2001, pp. 203–241.

[2]Salama, M., Kuo, C. P., and Lou, M., "Simulation of Deployment Dynamics of Inflatable Structures," *AIAA Journal*, Vol. 38, No. 12, 2000, pp. 2277–2283.

[3]Wang, J. T., and Johnson, A. R., "Deployment Simulation of Ultra-Lightweight Inflatable Structures," AIAA Paper 2002-1261, April 2002.

[4]Miyazaki, Y., and Uchiki, M., "Deployment Dynamics of Inflatable Tube," AIAA Paper 2002-1254, April 2002.

[5]Clem, A. L., Smith, S. W., and Main, J. A., "Deployment Dynamics of an Inflatable Solar Array," AIAA Paper 99-1520, April 1999.

[6]Clem, A. L., Smith, S. W., and Main, J. A., "A Pressurized Deployment Model for Inflatable Space Structures," AIAA Paper 2000-1808, April 2000.

[7]Clem, A. L., Smith, S. W., and Main, J. A., "Experimental Results Regarding the Inflation of Cylindrical Tubes," AIAA Paper 2001-1264, 2001.

[8]Smith, S. W., Elliott, M. D., Main, J. A., and Clem, A. L., "Post Flight Testing and Analysis of Zero-Gravity Deployment of an Inflating Tube," AIAA Paper 2001-1265, April 2001.

[9]Faugeras, O., *Three-Dimensional Computer Vision: A Geometric Viewpoint*, MIT Press, Cambridge, MA, 1993, pp. 33–68.

M. Lake
Associate Editor